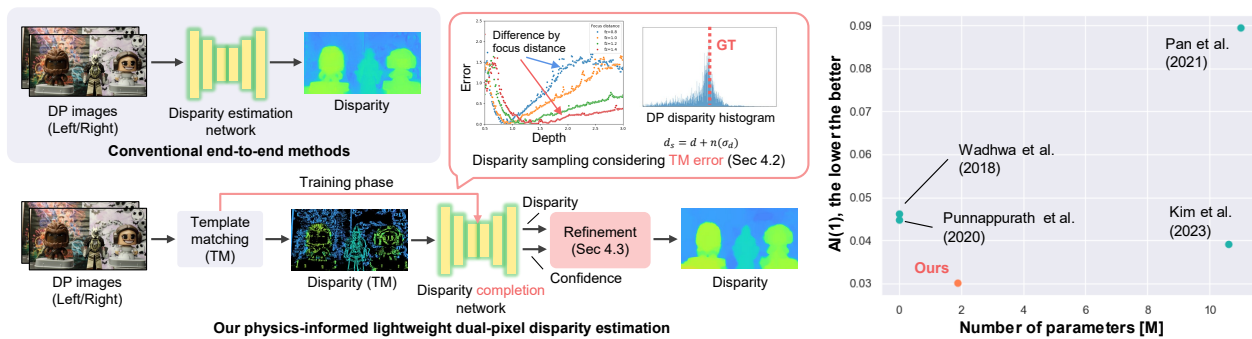


Revisiting Disparity from Dual-Pixel Images: Physics-Informed Lightweight Depth Estimation

Teppei Kurita Yuhi Kondo Legong Sun Takayuki Sasaki Sho Nitta
Yasuhiro Hashimoto Yoshinori Muramatsu Yusuke Moriuchi
Sony Semiconductor Solutions Corporation

{Teppei.Kurita, Yuhi.Kondo, Legong.Sun, Takayuki.Sasaki, Sho.Nitta,
Yasuhiro.Hashimoto, Yoshinori.Muramatsu, Yusuke.Moriuchi}@sony.com

<https://github.com/sony/dual-pixel-disparity>



(a) Comparison of proposed and conventional end-to-end methods

(b) Disparity estimation performance

Figure 1. **Overview of our method.** (a) Conventional end-to-end disparity or depth estimation from dual-pixel (DP) images is redundant and limited in performance because it does not exploit disparity constraints explicitly. The proposed method efficiently estimates disparity using a completion network trained to consider errors during template matching and a framework that refines the expansion of disparity regions that occur in principle. (b) shows the number of parameters on the horizontal axis and accuracy on the vertical axis; the closer to the lower left, the better the performance balance. The proposed method is lightweight and achieves high performance.

Abstract

In this study, we propose a high-performance disparity (depth) estimation method using dual-pixel (DP) images with few parameters. Conventional end-to-end deep-learning methods have many parameters but do not fully exploit disparity constraints, which limits their performance. Therefore, we propose a lightweight disparity estimation method based on a completion-based network that explicitly constrains disparity and learns the physical and systemic disparity properties of DP. By modeling the DP-specific disparity error parametrically and using it for sampling during training, the network acquires the unique properties of DP and enhances robustness. This learning also allows us to use a common RGB-D dataset for training without a DP dataset, which is labor-intensive to acquire. Furthermore, we propose a non-learning-based refinement framework that efficiently handles inherent disparity expansion errors by appropriately refining the confidence map of the network output. As a result, the proposed method achieved state-of-the-art results while reducing the overall system

size to 1/5 of that of the conventional method, even without using the DP dataset for training, thereby demonstrating its effectiveness. The code and dataset are available on our project site.

1. Introduction

Dual-pixel (DP) sensors [12, 21, 33, 36, 51] have traditionally been used for camera autofocus [10, 19]. This sensor splits each pixel into two photodiodes, providing two views of the same scene, as shown in Fig. 2 (b). The DP view has a disparity that correlates with the amount of defocus blur. Therefore, moving the lens position to minimize the disparity allows the scene to come into focus quickly. Similar to stereo cameras [4], the disparity can also be converted into depth, and the ease with which a depth map can be acquired without active-light illumination has led to its use in applications such as depth-of-field extension [1, 2, 47, 50] and segmentation [44]. Because of their affinity for these applications, DP sensors are utilized in mobile cameras, such as Google Pixel, which require lightweight systems.

Many techniques have been proposed for DP sensor disparity estimation; however, most of them use end-to-end estimation with deep learning, as shown at the top left of Fig. 1 (a). Although this method is simple and direct, it does not fully exploit the disparity constraint, which is highly reliable for disparity near textures. This unnecessarily increases the network size and limits performance; specifically, it is prone to disparity artifacts correlated with RGB textures, as shown in Fig. 9 (c). As a naïve solution, traditional template matching (TM) [7, 30] can explicitly calculate disparity only in regions of high reliability. A lightweight network optimized for completion can complement the disparity, thereby minimizing the network size and suppressing artifacts. However, the prominent anisotropic blurring property of DP outside the depth of field causes TM errors, which are further propagated by completion, resulting in degraded results. There is also the problem of disparity errors near the edges owing to the combination of lightweight completion networks, and the expansion of disparity in principle owing to TM, which causes the side effects of intermediate value disparity even when simple filter-based refinement processes are applied.

Therefore, we propose a physics-informed lightweight disparity estimation method that explicitly exploits the disparity property of DP, as shown at the bottom of Fig. 1 (a). Specifically, we propose an approach that improves accuracy by modeling the TM errors arising from the physical and systemic properties of DP and applying appropriate sampling during training. The physics DP simulator simulates varying optical conditions and fits parametric functions by using symbolic regression to efficiently model the TM errors. Furthermore, we propose a framework that effectively compensates for disparity expansion errors that occur in principle [15, 16] by carefully refining the network’s output confidence map based on a filtering process. The proposed non-learning-based disparity refinement framework is generally applicable and can be applied to the estimation results of other models.

In addition, a DP dataset is required to train the network; however, no dataset of DP images containing the actual disparity value exists to date [31]. Therefore, conventional methods use depth as a reference and learn by devising a loss function to absorb the differences in the domain. However, the network performance is limited by differences in the domain, and obtaining a large DP dataset with the ground truth of depth requires time and workforce, which are also limited in number and scale. By converting the depth of widely available monocular RGBD datasets to DP disparity, we enabled large-scale training in the same domain without needing large amounts of DP data.

The performance of the proposed method exceeds that of the state-of-the-art method by less than 1/5 of the parameters, demonstrating its superiority (Fig. 1(b)). In summary,

our contributions of this study are as follows:

- A practical method for estimating disparity (depth) from DP images in a lightweight and high-performance manner by modeling and appropriately constraining physics and systemic disparity properties. (Sec. 4.1, 4.2)
- A non-learning-based refinement framework that efficiently handles disparity expansion errors by appropriately refining the confidence map that network output (Sec. 4.3).
- An approach for learning disparity completion from common monocular RGBD data (Sec. 4.2).

2. Related works

Wadhwa et al. [44] first attempted to estimate the disparity between DP images obtained using DP sensors. They used stereo matching to calculate the disparity and stabilized it with bilateral smoothing. Punnappurath et al. [40] proposed a DP-specific point spread function (PSF) to reproduce the defocus blur that occurs in DP sensors. They employed an optimization process to obtain the depth estimation. However, these studies were based on simple filters, rule-based processing, and optimization, limiting their disparity or depth estimation performance. In recent years, end-to-end processing using deep learning has become mainstream, directly estimating disparity or depth from DP left and right images. Garg et al. [13] proposed a learning method that considers the indeterminacy inherent in DP. Pan et al. [37] proposed an unsupervised method that incorporated a physics DP simulator into the learning process. Kim et al. [24] proposed a loss function that considers DP-specific symmetries and achieved state-of-the-art performance by tuning a pretrained stereo network. Other studies have added new devices to DP sensors, such as coded-amplitude masks [14] and stereo cameras [52], to improve the accuracy. Although the deep-learning end-to-end processing used in these studies has shown impressive quantitative performance, it has limitations. This approach tends to increase the network size due to its inability to leverage the highly reliable disparity constraint near textures. Moreover, the internal processing of the network is a black box, which can lead to unexpected artifacts. Therefore, we propose an efficient and effective estimation method that explicitly exploits the disparity constraint and leverages the physical properties of DP.

3. Dual-pixel theory

3.1. Relation between disparity and depth

To understand how the disparity and depth generated by the DP sensor are related, consider imaging a point-light

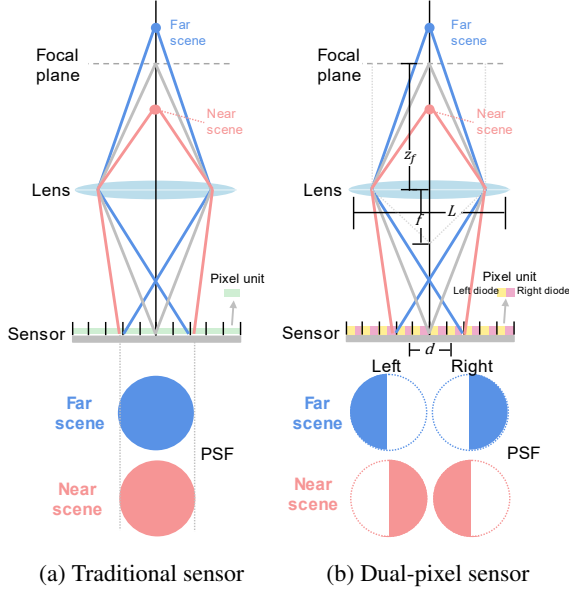


Figure 2. **PSF differences between traditional and DP sensors.** (a) With traditional sensors, the shape of the PSF is the same in both far and near scenes, and the same defocus blur occurs. (b) With the DP sensor, the PSF is shaded in the left and right halves of the left and right images, and its shape is inverted between the far and near scenes. This characteristic enables the DP sensor to calculate disparity by itself.

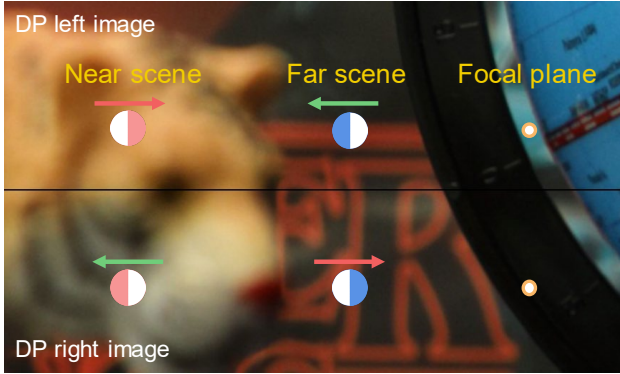


Figure 3. **Left and right images in a DP sensor.** The disparity generated by the DP sensor is small; however, the defocus blur is large. The PSF shape is different for left/right and perspective, making it more difficult to calculate disparity than when using a stereo camera.

source behind the focal plane and a point-light source in front of the focal plane in traditional and DP sensors, respectively, as shown in Fig. 2. For a point light source located farther from the focal plane (far scene), the light passes through the primary lens and comes into focus in front of the sensor, resulting in an out-of-focus image. For a point light source in front of the focal plane (near scene), the light passes through the primary lens and is focused behind

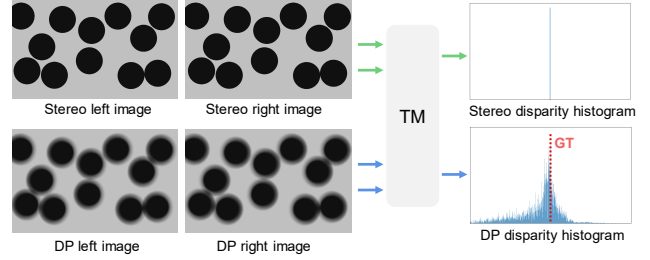


Figure 4. **Simulation of the difference between stereo and DP disparity calculation errors in the toy experiment.** Histograms of disparity were obtained by TM for stereo and DP images using a random dot chart, respectively. In stereo, the disparity is calculated accurately for most pixels; however, in DP, the disparity has many errors owing to the unique defocus blur.

the sensor, resulting in an out-of-focus image of the sensor. Using the traditional sensor shown in Fig. 2 (a), the PSF shape does not change for the far and near scenes and the same defocus blur is generated. In contrast, for the DP sensor, as shown in Fig. 2 (b), light passing through the left half of the primary lens aperture passes through the microlens at an angle that directs it toward the right half of the pixel and hits the right half of the pixel. Light passing through the right half of the lens hits the left half of the pixel in the opposite direction. Therefore, the PSF is shaded in the left and right halves, and its shape is inverted between the far and near scenes. The two images produced by the segmented pixels produce a defocus blur proportional to the aperture diameter L . The amount of blur is proportional to the disparity between the two images, and the final disparity d can be formulated as follows:

$$d = \alpha \frac{Lf}{1 - f/z_f} \left(\frac{1}{z_f} - \frac{1}{z} \right), \quad (1)$$

where z is the depth of the object, z_f is the focal distance, f is the focal length, and α is the proportionality constant. α can be obtained by calibrating the chart in advance. If the camera parameters are known, the depth can be obtained from the disparity.

3.2. Difficulty in calculating disparity in DP sensor

Figure 3 shows examples of the left and right images acquired by the DP sensor, arranged vertically. As shown in the figure, the disparity generated by the DP sensor is small because it is limited by the lens aperture L in Eqn. 1. As the disparity increases, the defocus blur also increases, and the shape of the PSF differs depending on whether it is left or right and on the perspective. Because of these properties, calculating disparity is more difficult for DP sensors than for stereo cameras.

To compare the difficulty of disparity calculation between stereo cameras and DP sensors, we performed a simple toy experiment, as shown in Fig. 4. We prepared random

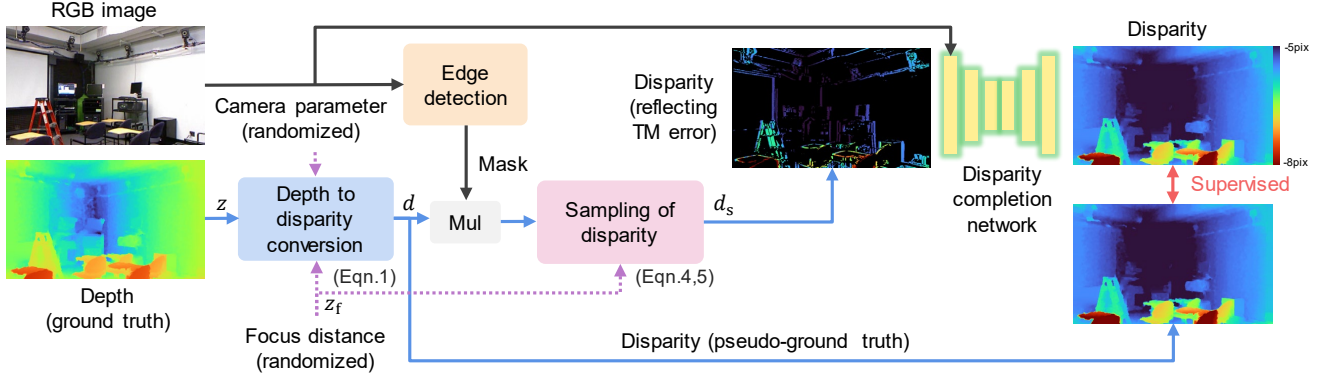


Figure 5. **Framework for learning disparity completion using RGBD data while incorporating the disparity properties of DP.** After converting the ground truth from depth to disparity and extracting only the edge portions, input disparity reflecting DP properties is generated by sampling to achieve supervised learning.

dot images from the stereo and DP cameras with the same ground-truth disparity. DP images were generated using a physics-based DP simulator with arbitrary camera parameter settings (see supplementary material). This simple example shows that TM can accurately calculate disparity for most pixels in standard stereo images. However, in DP, the disparity error is significant because of the unique defocus blur.

4. Method

4.1. Problem formulation

In recent years, as shown at the top left of Fig. 1 (a), the mainstream approach for disparity estimation in DP has been to learn a mapping $\mathcal{F} : \mathbf{I}_L, \mathbf{I}_R \rightarrow \hat{\mathbf{D}}$ such that disparity $\hat{\mathbf{D}}$ is directly estimated using the left and right images \mathbf{I}_L and \mathbf{I}_R of DP as inputs, as described in the following equation:

$$\hat{\mathbf{D}} = \mathcal{F}(\mathbf{I}_L, \mathbf{I}_R; \theta_{\mathcal{F}}), \quad (2)$$

where $\theta_{\mathcal{F}}$ are the weights to be learned.

In principle, the disparity cannot be calculated in textureless regions and must be complemented by estimating the disparity from the surrounding textured regions. However, end-to-end learning methods do not explicitly separate textured and nontextured regions, making the estimation process a black box. In many cases, the estimation results do not fully demonstrate the performance. Additionally, performing estimation in a single network tends to make it redundant and bloated.

As a naïve solution, assuming that the disparity is reliable in the region \mathbf{M} near the edge where the texture is present, the disparity can be explicitly calculated in that region using template matching \mathcal{T} . Disparity can then be complemented by referring to the image. The overview is shown at the bottom of Fig. 1 (a). Let $\mathcal{F}_c : \mathbf{D} \rightarrow \hat{\mathbf{D}}$ be the mapping from the sparse disparity \mathbf{D} to the dense disparity

$\hat{\mathbf{D}}$, as follows:

$$\hat{\mathbf{D}} = \mathcal{F}_c(\mathbf{D}, \mathbf{I}_L; \theta_{\mathcal{F}_c}), \quad \mathbf{D} = \mathbf{M} \odot \mathcal{T}(\mathbf{I}_L, \mathbf{I}_R). \quad (3)$$

An edge-extraction filter can determine the confidence region \mathbf{M} . By explicitly adding the disparity constraint, as in Eqn. 3, the process can be divided into two parts: one calculates the disparity \mathbf{D} of highly reliable texture regions, and the other uses reliable disparity \mathbf{D} as an input to complete the disparity $\hat{\mathbf{D}}$ of texture-free regions by referring to the RGB image \mathbf{I}_L . The problem setup for disparity completion is similar to that for depth completion, allowing the use of sophisticated and efficient depth completion networks [35, 42, 45, 46, 48], which have become increasingly competitive in recent years. However, if the learned model for depth completion is applied directly to disparity completion, the performance is limited by domain gaps. It would take considerable effort to obtain DP images containing the actual disparity value for training in the disparity domain, and no such dataset exists. Furthermore, as discussed in Sec. 3.2, errors in the disparity calculation of the DP sensor propagate throughout the completion process and thereby degrade the results.

4.2. Disparity completion learning reflecting DP property using RGBD data

Learning Framework Overview: We propose a physics-informed framework for learning disparity completion, as shown in Fig. 5, using widely available RGBD datasets such as NYUDv2 [41], while considering the physics and system properties of DP. First, the conversion in Eqn. 1 converts the ground truth from depth to disparity (which we define as pseudo-ground truth disparity), where the camera parameters are sampled randomly within a realistic range. The edge extraction filter described in Sec. 4.1 is applied to the RGB image, and only the edge regions of the generated ground truth disparity are extracted to reflect the disparity properties of DP by sampling, considering the TM error in

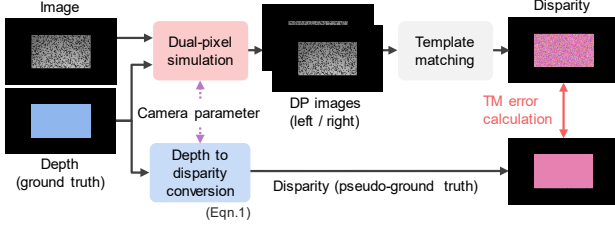


Figure 6. **Simulation for calculating TM errors in DP images.** Input random dot chart and ground truth depth, and generate DP left and right images by a physics simulation reflecting the optical properties of DP. Then, the disparity is calculated for the left and right images of DP by TM and compared with the pseudo-ground truth disparity to calculate the disparity error.

DP, which will be described later. In this case, the focus distance is the same as that in Eqn. 1. The network can be trained in a supervised manner using the disparity of the edge regions, which are generated as input and supervised by the pseudo-ground truth disparity.

Error simulation for sampling reflecting DP property:

We use a simulation to model the errors that occur in the TM of DP images. As shown in Fig. 6, the left and right DP images are generated by a physics simulation [3] reflecting the optical properties of DP in which a random dot chart and ground truth depth are prepared in CG, specific camera parameters such as focus distance and f-number are set, and the PSF kernel is convolved according to the depth values. The disparity is calculated for the generated left and right DP images by TM and then transformed from the depth of the ground truth to disparity using the same camera parameters from Eqn. 1 to obtain the disparity of pseudo-ground truth. The standard deviation of the disparity error is calculated by comparing the final calculated disparity with the pseudo-ground truth disparity. This procedure is used to simulate and acquire data under various conditions by changing the depth and camera parameters. Fig. 7 shows an example of the standard deviation of disparity at $f/2.0$. The error approaches zero when the depth is equivalent to the focus distance and tends to increase when front and rear focuses are used. We aim to model this standard deviation, which varies with the camera parameters, in an efficient and tractable form. We used PhySO [43], a symbolic regression method that employs reinforcement learning for parametric modeling, to obtain a model equation for the standard deviation σ_d of the disparity concerning depth in the following equation:

$$\sigma_d = c_1 \left(\frac{c_2 z}{F z_f} \right)^{\frac{z}{c_3}}, \quad (4)$$

where c_1, c_2 , and c_3 are constants, z is the depth of the ground truth, z_f is the focus distance, and F is the F value. This model equation is derived purely in a data-driven man-

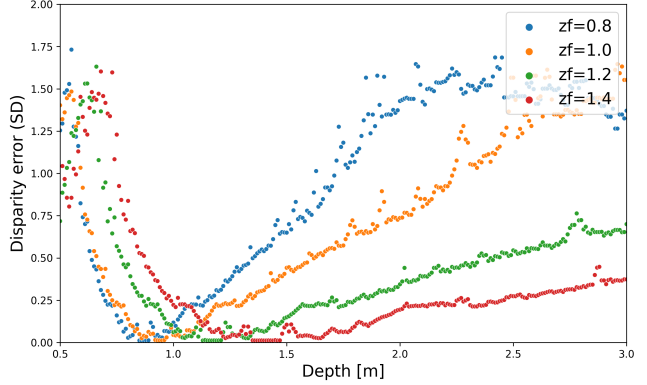


Figure 7. **Plots of TM error against depth for each focus distance.** The horizontal axis is the depth of the ground truth (z), and the vertical axis is the standard deviation of the disparity (σ_d), with colors indicating differences in focus distance (z_f). When the focus distance equals the depth, the error approaches zero, whereas the error increases for front focus and rear focus.

ner and has no specific physical basis. We use the Laplace distribution [28], which is the best-fitting probability distribution for the distribution of errors obtained from the toy experiments shown in Fig. 4 to generate the disparity error for DP. The final disparity is generated by adding an error term $n(\sigma_d)$ sampled from a zero-mean Laplace probability density function, as shown in the following equation:

$$d_s = d + n(\sigma_d) \quad (5)$$

where d is the input disparity, and d_s is the sampled disparity. This sampling can be used when training the disparity completion network to improve the completion accuracy because it reflects the TM error, which incorporates the DP's optical and system properties.

4.3. Disparity refinement considering confidence

In principle, calculating the disparity using TM expands the disparity regions depending on the window size [15, 16]. In the case of DP images, because of the inherent defocus blur, a large window size (approximately 30 pixels) is required for matching, resulting in an excessive expansion of the disparity region, as shown in Fig. 10 (c), Fig. 11 (b), and resulting in areas where the correct disparity cannot be calculated. Therefore, despite perfect estimation by the completion network described in Sec. 4.2, disparity errors will be significant near the edges. In recent years, neural networks for refinement have been studied extensively; however, the problem is that the entire system becomes bloated because additional parameters are required. For example, learning-based filtering methods, such as CSPN [9] and other refining methods [8, 20], require more than 10 million parameters. In addition, these methods exhibit limited performance for error types not included in the training data,

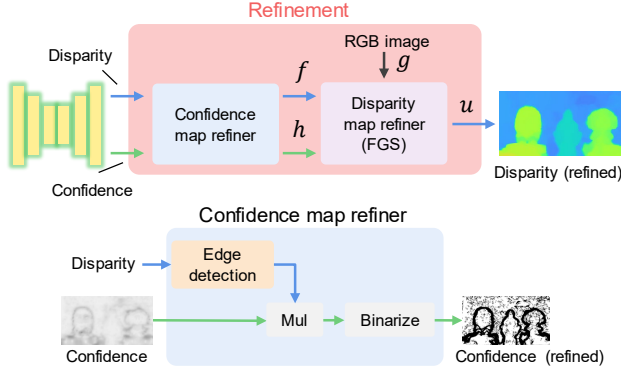


Figure 8. **Refinement framework for correcting disparity expansion errors that occur in principle in TM process.** Pre-processing is applied to the disparity and reliability for input to the FGS, which also considers the reliability of the network output to reduce the impact of errors and artifacts, thereby improving stability.

as observed in this case. However, there are widely known general-purpose refinement methods, such as the joint bilateral filter (JBF) [27] and guided filter (GF) [17], which do not require parameters. However, correcting a wide range of errors with a realistic kernel size is difficult, and preventing intermediate disparities is challenging.

Therefore, we focused on the fast global smoother (FGS) [34]. FGS can realize global optimization by combining 1D subsystems that reference neighboring pixels. It is suitable for efficiently refining a wide range of errors, such as colorization [29] and inpainting [6]. FGS is realized by solving the optimization problem expressed by the energy function in the following equation using a recursive filter:

$$J(u) = \sum_p \left(h_p(u_p - f_p)^2 + \lambda \sum_{q \in \mathcal{N}_4(p)} w_{p,q}(g)(u_p - u_q)^2 \right), \quad (6)$$

where p is a pixel, $\mathcal{N}_4(p)$ represents the four neighbors of p , u is the output data (refined disparity), f is the input data (disparity to be refined), h is the confidence map (binary) of the data term, and $w_{p,q}(g)$ is the similarity calculated from reference image g .

Figure 8 illustrates the proposed refinement framework. We propose improving the final disparity estimation performance by outputting the confidence map from the completion network and using it as a weight for the FGS. Hence, we use the uncertainty-depth joint optimization loss function [53] to learn the uncertainty map unsupervised (the disparity is learned supervised). The following equation expresses the loss function of the disparity completion network:

$$\mathcal{L} = \frac{1}{N} \sum \sqrt{e^{-s_i} (\hat{d}_i - d_i^{\text{gt}})^2 + 2s_i}, \quad (7)$$

$$s_i = 2 \log \sigma_i, \quad e^{s_i} = \sigma_i^2,$$

where d_i^{gt} is the ground truth disparity, \hat{d}_i is the complementary disparity, N is the number of pixels, and σ_i is the uncertainty map (inverted confidence map). As the uncertainty increases (lower confidence map), the agreement between the predictions and actual values is not required. Therefore, the learning process naturally leads to a lower confidence level in regions where variance is considered to be high. By learning the confidence map simultaneously, the network focuses on learning more appropriate features, thereby improving completion performance. The network configuration for outputting the confidence map is in the supplementary material. We assume that regions near edges where disparity expands have low confidence and propose using edge detection for the disparity to refine the confidence map. Specifically, the final confidence map is obtained by multiplying the edge detection results for the disparity output from the network by the initial confidence map and then binarizing to be input to the FGS. To obtain the effect of FGS with fewer iterations, noise reduction pre-processing, a weighted median filter [26, 32], is applied.

5. Experiment

5.1. Dataset and implementation details

We conducted several experiments to evaluate the proposed method. For the evaluation, we used the 100-pair DP dataset from Punnappurath et al. [40] and followed the same method used in previous studies to crop and evaluate the results. TM was performed using a simple sum of absolute differences (SAD) process with a window size of 27 pixels and a search range of ± 25 pixels. A mask for reliable disparity extraction was generated by applying a low-pass filter to the left image to suppress noise and then applying a process based on the Sobel filter [23]. The datasets used to train the disparity completion network included NYUDv2 [41] (1304 data points for training, 145 for validation), RGB-D-D [18] (4456 data points for training, 405 for validation), and our own CG data (9000 data points for training, 1000 for validation). Three different datasets are mixed, shuffled, and trained at each epoch to prevent bias. We used a network based on the cost volume-based depth completion network (CostDCNet) [22] with modifications, which is lightweight and performs well in terms of depth completion. The network architecture was implemented using PyTorch [39] on a PC with an NVIDIA A100 GPU. We trained the network for 50 epochs with a batch size of eight, Adam [25] as an optimizer, and an initial learning rate of 0.001. We then selected the model with the best validation results from the epoch. The constants in Eqn. 4, $c_1 = 6.93$, $c_2 = 0.48$, and $c_3 = 1.39$, were obtained by symbolic regression.

Table 1. Disparity evaluation for each method on [40] dataset.

| Method | AI(1)↓ | AI(2)↓ | $1 - \rho_s \downarrow$ | Param |
|-------------------|---------------|---------------|---------------------------|------------|
| Wadhwa [44] | 0.0463 | 0.0740 | 0.2875 | $\simeq 0$ |
| Punnappurath [40] | 0.0449 | 0.0724 | 0.2301 | $\simeq 0$ |
| Pan [37] | 0.0894 | 0.1491 | 0.5008 | 11.0M |
| Kim [24] | 0.0390 | 0.0679 | 0.2092 | 10.6M |
| Ours | 0.0301 | 0.0667 | 0.0782 | 1.9M |

5.2. Assessment

As in existing studies [24, 37, 40], the affine invariant metric $AI(p)$, calculated between the estimated disparity and the inverse depth of the ground truth, is used for evaluation. $AI(p)$ is defined as follows:

$$AI(p) = \operatorname{argmin}_{\beta_0, \beta_1} \left(\frac{1}{N} \sum |d_i^{\text{gt}} - (\beta_0 + \beta_1 \hat{d}_i)|^p \right)^{1/p}, \quad (8)$$

where d_i^{gt} is the inverse depth map of the ground truth, \hat{d}_i is the estimated disparity, and β_0 and β_1 are the optimized affine coefficients. The mean absolute error (MAE) for $p = 1$ and the root mean squared error (RMSE) for $p = 2$, with lower values indicating higher accuracy. As in existing studies, we also evaluated $1 - |\rho_s|$ using Spearman’s rank correlation coefficient between d_i^{gt} and \hat{d}_i transformed using the optimized affine coefficients. In this measure, the lower the value, the higher is the rank correlation between the two datasets. Furthermore, the number of parameters in the network is simultaneously reported.

Comparison with conventional methods: We compared our method with four other DP estimation methods: Wadhwa et al. [44], Punnappurath et al. [40], Pan et al. [37], and Kim et al. [24]. Wadhwa et al. [44] used stereo matching followed by bilateral smoothing to obtain the disparity. The other three methods directly obtain the disparity from DP images using an optimization process [40] or a neural network [24, 37]. The results summarized in Tab. 1 show that our method outperforms existing methods in the three evaluation metrics. The number of parameters is also less than 1/5 of other neural network-based methods, indicating that a lightweight and highly accurate estimation can be performed. Figure 1(b) plots the number of parameters on the horizontal axis and performance on the vertical axis. The closer to the lower left of the graph, the fewer the parameters and the better the performance, showing that our method achieves high performance while maintaining a low number of parameters. Figure 9 shows the results of the qualitative comparison. The results show that Kim et al.’s end-to-end method generates false disparities in planes with uniform disparity (depth), such as walls. In contrast, our method does not produce such artifacts because it appropriately complements reliable disparities while considering

Table 2. Ablation study.

| Measure | AI(1)↓ | AI(2)↓ | $1 - \rho_s \downarrow$ |
|-------------------------------|---------------|---------------|---------------------------|
| Baseline (DC network) | 0.0477 | 0.0812 | 0.1436 |
| + (1) Sec 4.2 | 0.0476 | 0.0825 | 0.1427 |
| + (2) Sec 4.2 w/ Eqn. 4, 5 | 0.0381 | 0.0704 | 0.1121 |
| + (3) Sec 4.3 | 0.0317 | 0.0684 | 0.0816 |
| + (4) Sec 4.3 w/ conf refiner | 0.0301 | 0.0667 | 0.0782 |

Table 3. Comparison of refinement methods.

| Method | Type | AI(1)↓ | AI(2)↓ | $1 - \rho_s \downarrow$ |
|----------------|-----------|---------------|---------------|---------------------------|
| w/o refinement | - | 0.0381 | 0.0704 | 0.1121 |
| JBF [27] | Filtering | 0.0365 | 0.0668 | 0.1121 |
| GF [17] | Filtering | 0.0355 | 0.0636 | 0.1005 |
| FBS [5] | Filtering | 0.0378 | 0.0699 | 0.2302 |
| TGV [11] | Prior | 0.0368 | 0.0666 | 0.1041 |
| AR [49] | Prior | 0.0377 | 0.0697 | 0.2858 |
| CSPN [9] | Learning | 0.0380 | 0.0698 | 0.1130 |
| Ours | Filtering | 0.0301 | 0.0667 | 0.0782 |

DP properties. In addition, our method generates sharper results even at the edges of the disparities without generating intermediate disparities.

Ablation study: Table 2 presents the results of an ablation study confirming the effectiveness of the proposed method. The baseline directly uses a depth completion (DC) network trained on RGBD data to complete the disparity. In (1), the conversion from depth to disparity described in Sec. 4.2 using Eqn. 1 is performed during training. In (2), in addition to (1), sampling is performed during training to reproduce the disparity error in template matching of DP images using Eqn. 4, 5 in Sec. 4.2. In (3), the refinement process of the disparity expansion error described in Sec. 4.3 is added to (1) and (2). In (4), the confidence map refinement and pre-processing are performed in addition to (1), (2), and (3). The effectiveness of each measure was confirmed, and as can be seen from the results in (2), even without the refinement process of the disparity expansion error, this method performs as well as or better than the conventional methods in Tab. 1.

Comparison with disparity expansion errors refinement: Table 3 shows how the effectiveness of our proposed framework for correcting disparity expansion errors compares to filter-based methods like JBF [27], GF [17] and fast bilateral solver (FBS) [5], prior knowledge (model)-based optimization methods like the total generalized variation (TGV) [11] and adaptive autoregressive model (AR) [49], and the learning-based method convolutional spatial propagation network (CSPN) [9]. We integrated the CSPN after our completion network and trained it simul-

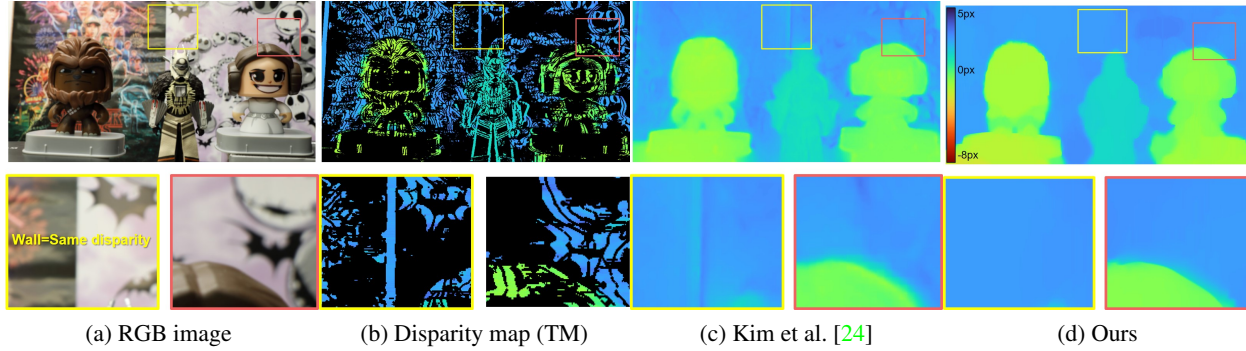


Figure 9. **Qualitative comparison of our results with other methods.** Kim et al.’s end-to-end method [24] produces false disparity in planes with uniform disparity (depth), such as walls. In contrast, our method does not generate such artifacts.

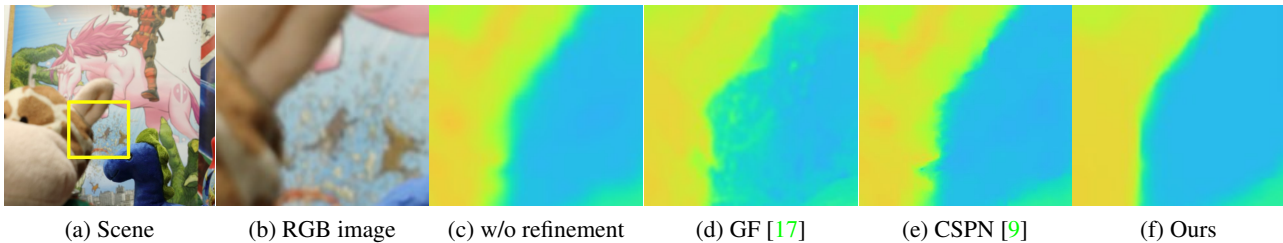


Figure 10. **Qualitative comparison of refinement methods.** GF produces intermediate disparity values correlated to the wall textures; however, our method does not produce such artifacts. Our method also has more precise boundary areas than the learning-based CSPN.

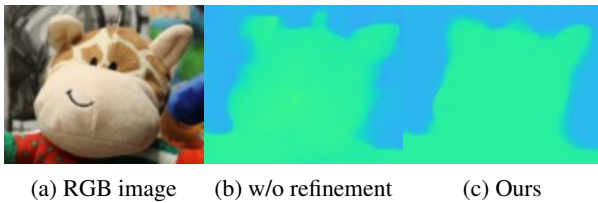


Figure 11. **Proposed refinement framework can be applied generically to other networks.** (b) Results of using NLSPN [38], a model with more parameters, as a completion model. (c) Result of applying our proposed framework to (b).

taneously within the framework shown in Fig. 5. The results of these correction methods demonstrate the high accuracy of the proposed method. For AI(2), GF was the best, however, the qualitative results in Fig. 10 show that the GF results exhibit a significant intermediate disparity around the edges, whereas the proposed method exhibits no such side effects and is stable. Learning-based methods, such as CSPN, exhibit limited performance in situations in which unexpected errors (disparity regions magnified by TM) are not included during training.

Apply our refinement framework to other disparity estimation models: The proposed disparity refinement framework is sufficiently versatile to be applied to the disparity estimation results in other models. Fig. 11 shows the results obtained by using a non-local spatial propagation network (NLSPN) [38], which is a model that has more parameters than does CostDCNet, as a completion model and

applying our disparity refinement framework. Even with a richer model, there is still some instability around the disparity edges. However, the refinement process can still estimate the disparity with high accuracy. Please refer to the supplementary material for detailed comparative results, including the network configuration for outputting confidence in the NLSPN and for quantitative evaluation.

6. Discussions and conclusion

This study proposes a low-parameter and highly accurate method for disparity (depth) estimation from DP images. Compared to conventional end-to-end processing, the proposed method is easy to implement in hardware because each processing phase and purpose are clearly separated. The development of this field will improve the accuracy of the depth obtained from the DP sensor and expand its range of applications. We will further study this method for future applications when an increasing number of cameras are equipped with a DP sensor.

Limitations: In this study, to make a fair comparison with existing studies, an evaluation was performed on a specific dataset, and a detailed evaluation of data obtained in other settings (lens aperture, focal length, etc.) was not performed. The proposed method assumes and assigns various optical parameters when considering DP properties, and we confirmed that it is qualitatively adequate on our own dataset (see supplementary material). A more exhaustive evaluation will be the subject of future studies.

References

- [1] Abdullah Abuolaim, Mahmoud Afifi, and Michael S Brown. Improving single-image defocus deblurring: How dual-pixel images help through multi-task learning. In Proceedings of the IEEE/CVF Winter Conference on Applications of Computer Vision (WACV), pages 1231–1239, 2022. 1
- [2] Abdullah Abuolaim and Michael S Brown. Defocus deblurring using dual-pixel data. In European Conference on Computer Vision (ECCV), pages 111–126. Springer, 2020. 1
- [3] Abdullah Abuolaim, Mauricio Delbracio, Damien Kelly, Michael S Brown, and Peyman Milanfar. Learning to reduce defocus blur by realistically modeling dual-pixel data. In Proceedings of the IEEE/CVF International Conference on Computer Vision (ICCV), pages 2289–2298, 2021. 5
- [4] Stephen T Barnard and Martin A Fischler. Computational stereo. ACM Computing Surveys (CSUR), 14(4):553–572, 1982. 1
- [5] Jonathan T Barron and Ben Poole. The fast bilateral solver. In European conference on computer vision, pages 617–632. Springer, 2016. 7
- [6] Marcelo Bertalmio, Guillermo Sapiro, Vincent Caselles, and Coloma Ballester. Image inpainting. In Proceedings of the 27th Annual Conference on Computer Graphics and Interactive Techniques, pages 417–424, 2000. 6
- [7] Roberto Brunelli. Template matching techniques in computer vision: theory and practice. John Wiley & Sons, 2009. 2
- [8] Xinjing Cheng, Peng Wang, Chenye Guan, and Ruigang Yang. CSPN++: Learning context and resource aware convolutional spatial propagation networks for depth completion. In Proceedings of the AAAI Conference on Artificial Intelligence, volume 34, pages 10615–10622, 2020. 5
- [9] Xinjing Cheng, Peng Wang, and Ruigang Yang. Depth estimation via affinity learned with convolutional spatial propagation network. In European Conference on Computer Vision (ECCV), pages 103–119, 2018. 5, 7, 8
- [10] Myungsub Choi, Hana Lee, and Hyong-euk Lee. Exploring positional characteristics of dual-pixel data for camera autofocus. In Proceedings of the IEEE/CVF International Conference on Computer Vision (ICCV), pages 13158–13168, 2023. 1
- [11] David Ferstl, Christian Reinbacher, Rene Ranftl, Matthias R  ther, and Horst Bischof. Image guided depth upsampling using anisotropic total generalized variation. In Proceedings of the IEEE/CVF International Conference on Computer Vision (ICCV), pages 993–1000, 2013. 7
- [12] Ray Fontaine. The state-of-the-art of mainstream cmos image sensors. In Proceedings of the International Image Sensors Workshop, pages 6–12. IISW, 2015. 1
- [13] Rahul Garg, Neal Wadhwa, Sameer Ansari, and Jonathan T Barron. Learning single camera depth estimation using dual-pixels. In Proceedings of the IEEE/CVF International Conference on Computer Vision (ICCV), pages 7628–7637, 2019. 2
- [14] Bhargav Ghanekar, Salman Siddique Khan, Vivek Boominathan, Pranav Sharma, Shreyas Singh, Kaushik Mitra, and Ashok Veeraraghavan. Passive snapshot coded aperture dual-pixel RGB-D imaging. arXiv preprint arXiv:2402.18102, 2024. 2
- [15] Raj Kumar Gupta and Siu-Yeung Cho. Window-based approach for fast stereo correspondence. IET Computer Vision, 7(2):123–134, 2013. 2, 5
- [16] Rostam Affendi Hamzah and Haidi Ibrahim. Literature survey on stereo vision disparity map algorithms. Journal of Sensors, 2016(1):8742920, 2016. 2, 5
- [17] Kaiming He, Jian Sun, and Xiaoou Tang. Guided image filtering. IEEE Transactions on Pattern Analysis and Machine Intelligence (TPAMI), 35(6):1397–1409, 2012. 6, 7, 8
- [18] Lingzhi He, Hongguang Zhu, Feng Li, Huihui Bai, Runmin Cong, Chunjie Zhang, Chunyu Lin, Meiqin Liu, and Yao Zhao. Towards fast and accurate real-world depth super-resolution: Benchmark dataset and baseline. In Proceedings of the IEEE/CVF Conference on Computer Vision and Pattern Recognition (CVPR), pages 9229–9238, 2021. 6
- [19] Charles Herrmann, Richard Strong Bowen, Neal Wadhwa, Rahul Garg, Qiurui He, Jonathan T Barron, and Ramin Zabih. Learning to autofocus. In Proceedings of the IEEE/CVF Conference on Computer Vision and Pattern Recognition (CVPR), pages 2230–2239, 2020. 1
- [20] Mu Hu, Shuling Wang, Bin Li, Shiyu Ning, Li Fan, and Xiaojin Gong. PENet: Towards precise and efficient image guided depth completion. In IEEE International Conference on Robotics and Automation (ICRA), pages 13656–13662. IEEE, 2021. 5
- [21] Taesub Jung, Masato Fujita, Jeongjin Cho, Kyungduck Lee, Doosik Seol, Sungmin An, Chanhee Lee, Youjin Jeong, Minji Jung, Sachoun Park, et al. A 1/1.57-inch 50mpixel CMOS image sensor with 1.0 μm all-directional dual pixel by 0.5 μm -pitch full-depth deep-trench isolation technology. In IEEE International Solid-State Circuits Conference (ISSCC), volume 65, pages 102–104. IEEE, 2022. 1
- [22] Jaewon Kam, Jungeon Kim, Soongjin Kim, Jaesik Park, and Seungyong Lee. CostDCnet: Cost volume based depth completion for a single RDB-D image. In European Conference on Computer Vision (ECCV), pages 257–274. Springer, 2022. 6
- [23] Nick Kanopoulos, Nagesh Vasanthavada, and Robert L Baker. Design of an image edge detection filter using the sobel operator. IEEE Journal of Solid-state Circuits, 23(2):358–367, 1988. 6
- [24] Donggun Kim, Hyeonjoong Jang, Inchul Kim, and Min H Kim. Spatio-focal bidirectional disparity estimation from a dual-pixel image. In Proceedings of the IEEE/CVF Conference on Computer Vision and Pattern Recognition (CVPR), pages 5023–5032, 2023. 2, 7, 8
- [25] Diederik P Kingma and Jimmy Ba. Adam: A method for stochastic optimization. arXiv preprint arXiv:1412.6980, 2014. 6
- [26] S-J Ko and Yong Hoon Lee. Center weighted median filters and their applications to image enhancement. IEEE Transactions on Circuits and Systems, 38(9):984–993, 1991. 6

- [27] Johannes Kopf, Michael F Cohen, Dani Lischinski, and Matt Uyttendaele. Joint bilateral upsampling. *ACM Transactions on Graphics (ToG)*, 26(3):96–es, 2007. 6, 7
- [28] Samuel Kotz, Tomasz Kozubowski, and Krzysztof Podgorski. *The Laplace distribution and generalizations: a revisit with applications to communications, economics, engineering, and finance*. Springer Science & Business Media, 2012. 5
- [29] Anat Levin, Dani Lischinski, and Yair Weiss. Colorization using optimization. In *ACM SIGGRAPH 2004 Papers*, pages 689–694. 2004. 6
- [30] John P Lewis et al. Fast template matching. In *Vision Interface*, volume 95, pages 15–19. Quebec City, QC, Canada, 1995. 2
- [31] Feiran Li, Heng Guo, Hiroaki Santo, Fumio Okura, and Yasuyuki Matsushita. Learning to synthesize photorealistic dual-pixel images from RGBD frames. In *IEEE International Conference on Computational Photography (ICCP)*, pages 1–11. IEEE, 2023. 2
- [32] Ziyang Ma, Kaiming He, Yichen Wei, Jian Sun, and Enhua Wu. Constant time weighted median filtering for stereo matching and beyond. In *Proceedings of the IEEE/CVF International Conference on Computer Vision (ICCV)*, pages 49–56, 2013. 6
- [33] W Machado et al. Canon LC1290A (die markings) 20.2 Mp, 4.1 μm pixel size dual pixel CMOS AF APS-C CMOS image sensor from the Canon EOS-70D (W) DSLR camera imager process review. *Chipworks*, October, 2013. 1
- [34] Dongbo Min, Sunghwan Choi, Jiangbo Lu, Bumsub Ham, Kwanghoon Sohn, and Minh N Do. Fast global image smoothing based on weighted least squares. *IEEE Transactions on Image Processing (TIP)*, 23(12):5638–5653, 2014. 6
- [35] Danish Nazir, Alain Pagani, Marcus Liwicki, Didier Stricker, and Muhammad Zeshan Afzal. Semattnet: Toward attention-based semantic aware guided depth completion. *IEEE Access*, 10:120781–120791, 2022. 4
- [36] Tetuya Okawa, Susumu Ooki, Hiroaki Yamajo, Masakazu Kawada, Masayuki Tachi, Kazuhiro Goi, Takatsugu Yamasaki, Hiroki Iwashita, Masahiko Nakamizo, Takayuki Ogasahara, et al. A 1/2inch 48M all PDAF CMOS image sensor using 0.8 μm quad bayer coding $2\times 2\text{oCL}$ with 1.0 lux minimum AF illuminance level. In *IEEE International Electron Devices Meeting (IEDM)*, pages 16–3. IEEE, 2019. 1
- [37] Liyuan Pan, Shah Chowdhury, Richard Hartley, Miaomiao Liu, Hongguang Zhang, and Hongdong Li. Dual pixel exploration: Simultaneous depth estimation and image restoration. In *Proceedings of the IEEE/CVF Conference on Computer Vision and Pattern Recognition (CVPR)*, pages 4340–4349, June 2021. 2, 7
- [38] Jinsun Park, Kyungdon Joo, Zhe Hu, Chi-Kuei Liu, and In So Kweon. Non-local spatial propagation network for depth completion. In *European Conference on Computer Vision (ECCV)*, pages 120–136. Springer, 2020. 8
- [39] Adam Paszke, Sam Gross, Francisco Massa, Adam Lerer, James Bradbury, Gregory Chanan, Trevor Killeen, Zeming Lin, Natalia Gimelshein, Luca Antiga, et al. Pytorch: An imperative style, high-performance deep learning library. *Advances in Neural Information Processing Systems*, 32, 2019. 6
- [40] Abhijith Punnappurath, Abdullah Abuolaim, Mahmoud Afifi, and Michael S Brown. Modeling defocus-disparity in dual-pixel sensors. In *IEEE International Conference on Computational Photography (ICCP)*, pages 1–12. IEEE, 2020. 2, 6, 7
- [41] Nathan Silberman, Derek Hoiem, Pushmeet Kohli, and Rob Fergus. Indoor segmentation and support inference from RGBD images. In *European Conference on Computer Vision (ECCV)*, pages 746–760. Springer, 2012. 4, 6
- [42] Jie Tang, Fei-Peng Tian, Boshi An, Jian Li, and Ping Tan. Bilateral propagation network for depth completion. In *Proceedings of the IEEE/CVF Conference on Computer Vision and Pattern Recognition (CVPR)*, pages 9763–9772, 2024. 4
- [43] Wassim Tenachi, Rodrigo Ibata, and Foivos I Diakogiannis. Deep symbolic regression for physics guided by units constraints: toward the automated discovery of physical laws. *The Astrophysical Journal*, 959(2):99, 2023. 5
- [44] Neal Wadhwa, Rahul Garg, David E Jacobs, Bryan E Feldman, Nori Kanazawa, Robert Carroll, Yair Movshovitz-Attias, Jonathan T Barron, Yael Pritch, and Marc Levoy. Synthetic depth-of-field with a single-camera mobile phone. *ACM Transactions on Graphics (ToG)*, 37(4):1–13, 2018. 1, 2, 7
- [45] Yufei Wang, Bo Li, Ge Zhang, Qi Liu, Tao Gao, and Yuchao Dai. Lrru: Long-short range recurrent updating networks for depth completion. In *Proceedings of the IEEE/CVF International Conference on Computer Vision (ICCV)*, pages 9422–9432, 2023. 4
- [46] Yufei Wang, Ge Zhang, Shaoqian Wang, Bo Li, Qi Liu, Le Hui, and Yuchao Dai. Improving depth completion via depth feature upsampling. In *Proceedings of the IEEE/CVF Conference on Computer Vision and Pattern Recognition (CVPR)*, pages 21104–21113, 2024. 4
- [47] Shumian Xin, Neal Wadhwa, Tianfan Xue, Jonathan T Barron, Pratul P Srinivasan, Jiawen Chen, Ioannis Gkioulekas, and Rahul Garg. Defocus map estimation and deblurring from a single dual-pixel image. In *Proceedings of the IEEE/CVF International Conference on Computer Vision (ICCV)*, pages 2228–2238, 2021. 1
- [48] Zhiqiang Yan, Kun Wang, Xiang Li, Zhenyu Zhang, Jun Li, and Jian Yang. RigNet: Repetitive image guided network for depth completion. In *European Conference on Computer Vision (ECCV)*, pages 214–230. Springer, 2022. 4
- [49] Jingyu Yang, Xinchun Ye, Kun Li, Chunping Hou, and Yao Wang. Color-guided depth recovery from RGB-D data using an adaptive autoregressive model. *IEEE Transactions on Image Processing (TIP)*, 23(8):3443–3458, 2014. 7
- [50] Yan Yang, Liyuan Pan, Liu Liu, and Miaomiao Liu. K3DN: Disparity-aware kernel estimation for dual-pixel defocus deblurring. In *Proceedings of the IEEE/CVF Conference on Computer Vision and Pattern Recognition (CVPR)*, pages 13263–13272, 2023. 1
- [51] Sukki Yoon, Jungbin Yun, Yunhwan Jung, Ilyun Jeong, Junghee Choi, Wooseok Choi, Jeongguk Lee, Hansoo Lee,

and Juhyun Ko. World largest mobile image sensor with all directional phase detection auto focus function. In IEEE Hot Chips 33 Symposium (HCS), pages 1–22. IEEE, 2021. [1](#)

- [52] Yinda Zhang, Neal Wadhwa, Sergio Orts-Escolano, Christian Häne, Sean Fanello, and Rahul Garg. Du²Net: Learning depth estimation from dual-cameras and dual-pixels. In European Conference on Computer Vision (ECCV), pages 582–598. Springer, 2020. [2](#)
- [53] Yufan Zhu, Weisheng Dong, Leida Li, Jinjian Wu, Xin Li, and Guangming Shi. Robust depth completion with uncertainty-driven loss functions. In Proceedings of the AAAI Conference on Artificial Intelligence, volume 36, pages 3626–3634, 2022. [6](#)